IEEE Access
Multidisciplinary | Rapid Review | Open Access Journal

Received 27 May 2023, accepted 10 June 2023, date of publication 13 June 2023, date of current version 19 June 2023.

Digital Object Identifier 10.1109/ACCESS.2023.3285774

RESEARCH ARTICLE

Analysis of High Gain Wideband 2 × 2 Printed Slot Array With AMC Surface by Presenting Equivalent Transmission Line Model for C and X-Band Applications

HOSSEIN MALEKPOOR[1], (Member, IEEE), AND MEHDI HAMIDKHANI[2,3]

[1]Department of Electrical Engineering, Faculty of Engineering, Arak University, Arak 38156-8-8349, Iran
[2]Department of Electrical Engineering, Dolatabad Branch, Islamic Azad University, Isfahan 8341875185, Iran
[3]Department of Electrical Engineering, Isfahan (khorasgan) Branch, Islamic Azad University, Isfahan 1477893855, Iran

Corresponding author: Hossein Malekpoor (h-malekpoor@araku.ac.ir)

ABSTRACT A low-profile broadband 2 × 2 printed slot array with V-shaped slots by loading broadband artificial magnetic conductor (AMC) is demonstrated. A proposed wideband printed array with tapered V-shaped slots with the feeding of coplanar-waveguide (CPW) is measured in 8.24-11.13 GHz. Also, the proposed wideband planar AMC surface is embedded into the printed array to attain enhanced radiation properties. The printed slot array with the 7 × 7 AMC surface covers -10 dB measured bandwidth from 4.47 to 13.32 GHz (100%). The design loaded by AMC compared to the design without AMC introduces a reduced size of 109.4%, a bandwidth improvement of 70%, and good impedance matching. Moreover, by adding an AMC surface into the printed array, an enhanced gain of 12.3 dBi with uni-directional radiation patterns is attained. The measured gain over the wide bandwidth shows acceptable stability with an average gain of almost 11 dBi. The proposed AMC unit cell is proposed to resonate at 10.10 GHz with a bandwidth of 7.85-12.24 GHz (43.7%) for X-band applications. In addition, the proposed equivalent transmission line model of the antenna with AMC is presented with acceptable output results. This model forecasts the input impedance of the printed array with AMC at the frequency band of 4.50-13.30 GHz as well.

INDEX TERMS AMC, V-shaped slot, printed slot antenna, wideband, equivalent transmission line model.

I. INTRODUCTION

Most modern wireless networks have utilized electromagnetic band gap (EBG) structures for broadband networks due to their significant and unique characteristics. These structures conclude the conditions of high-impedance surfaces and, consequently, abolish surface waves [1]. The artificial magnetic conductor (AMC) structures show the same performance as a perfect magnetic conductor. In this regard, the image elements for PMCs are in-phase with the primary element that allocates applying those as reflectors in antennas. Also, it concludes placing the radiating elements very nearby to the PMC, which leads to low-profile antennas. In the recent decade, many low-profile antennas with AMC surfaces are introduced with the prominent outputs [2], [3], [4], [5], [6], [7], [8], [9], [10]. The broadband patch arrays by inserting various EBG-AMCs are reported in [9].

Nowadays, by extending the wireless networks and communications, microstrip patch antennas have been taken into account in several research works. It is due to important features of a simple fulfillment, low-profile antenna, and light weight. In reported works many approaches have been carried out to enlarge the bandwidth of microstrip antennas [11]. Wireless systems have an excellent data rate transmission, and coating multipath circumstance, and hence, low-profile wideband microstrip antennas are paid attention for related applications [12], [13], [14], [15]. Various EBG surfaces for WLAN systems have been used with their attractive features [14]. In this regard, several compact antennas are used

The associate editor coordinating the review of this manuscript and approving it for publication was Bilal Khawaja.

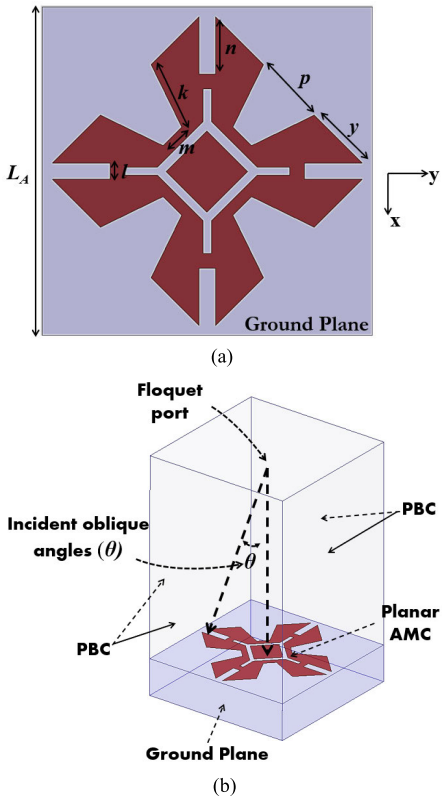

FIGURE 1. (a) AMC design and (b) Infinite box with boundary condition.

AMC surfaces to promote the radiation properties [16], [17], [18], [19], [20], [21], [22], [23].

It is important to notice that AMCs have a narrow bandwidth to apply in the broadband microwave circuits and printed antennas [24]. In the most works, different types of microstrip antennas backed by wideband AMC surfaces are used with enhancement results by realizing the printed circuit technologies [25], [26], [27], [28], [29], [30], [31], [32], [33], [34], [35], [36], [37], [38], [39]. A printed antenna with AMC in [34] reports a measured bandwidth of 18% in 2.2-2.72 GHz with sizes of 67.5 × 67.5 × 4.5 mm^3. In [37], a low-profile flexible dual-band and dual-CP with the AMC surfaces is realized to achieve a broadband antenna at 3.5 and 5.8 GHz (11.7%) with a higher gain of 7.2 dBi.

This study reports a wideband printed slot array with the AMC surface. A wideband AMC unit cell is presented to resonate at 10.10 GHz (7.85-12.24 GHz), firstly. By loading the 7 × 7 AMC periodic surface, the low-profile wideband printed array is realized. The 2 × 2 printed array includes four tapered V-shaped slots and a CPW feeding system to expand the bandwidth for X-band. Consequently, a broadband AMC reflector is located beneath the antenna to measure the −10 dB bandwidth in 4.47-13.32 GHz (100%) and an increased gain of 12.3 dBi. Eventually, the equivalent transmission line model is prepared to anticipate the input impedance of the printed array with AMC surface.

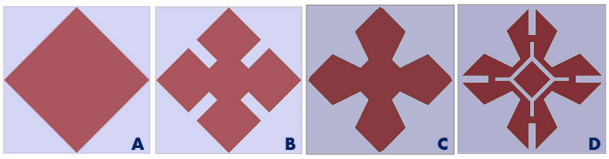

FIGURE 2. Design evolution of AMC.

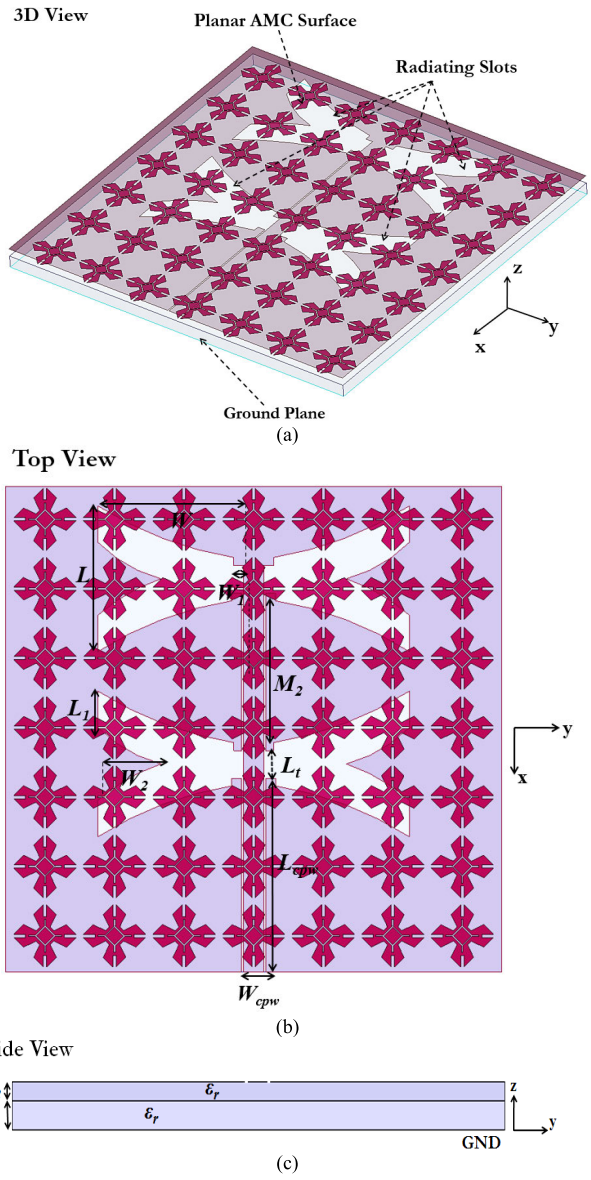

FIGURE 3. Antenna with the 7 × 7 AMC (a) 3D view (b) top view (c) side view.

II. PRINTED 2 × 2 SLOT ARRAY WITH AMC STRUCTURE

A. SUGGESTED AMC SURFACE

Fig. 1 displays the structure of a proposed AMC unit cell. The relative permittivity and thickness of $\varepsilon_r = 4.4$ and $h_1 = 2.1$ mm, respectively are selected for the utilized substrate of FR4. The dimensions of the unit cell and ground plane are 10.3×10.3 mm^2 and 11.3×11.3 mm^2, respectively. The AMC is simulated by utilizing the finite element method for periodic structures to calculate the AMC reflection

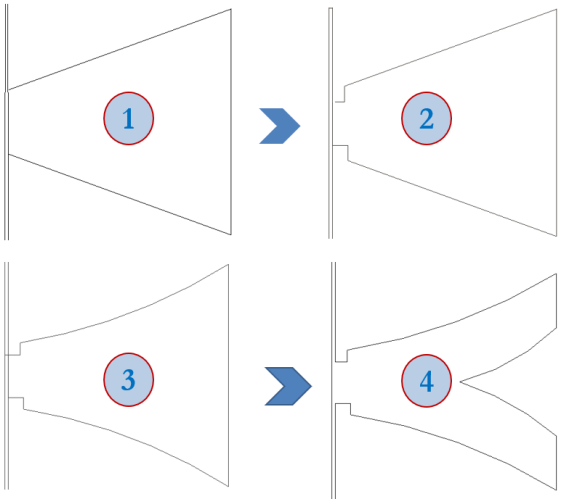

FIGURE 4. Design evolution of printed slot antenna.

TABLE 1. Sizes of the antenna with AMC.

Parameters	Values (mm)
W	24
W_1	0.3
W_2	11.3
L_1	5
L_t	5.1
L_{cpw}	30.4
W_{cpw}	3
h_1	2.1
h_2	1.6
m	1.1
k	3.7
p	3.5
y	3

coefficients with a periodic boundary condition as shown in Fig. 1 (b).

The bandwidth improvement of the AMC is concluded from the physical and electrical characteristics. The effective couplings of slots and arms result in the physical specification of the wide bandwidth. The optimal AMC bandwidth is obtained by selecting the given electrical characteristic of h and ε_r. Eventually, various scan angles of reflection waves are investigated with proper stability for a wideband operation. Indeed, different parts and inserted slots into the AMC surface lead to a wider bandwidth.

The mushroom-type EBG structure is composed by a via-loaded patch with an equivalent parallel LC model of $f_r = 1/(2\pi\sqrt{LC})$ [18]. The L and C parameters, and impedance bandwidth are determined by the bellow equations [18]:

$$C = \frac{W_{ebg}\varepsilon_0(1+\varepsilon_r)}{\pi}\cosh^{-1}\left(\frac{2W_{ebg}+g}{g}\right) \quad (1)$$

$$L = \mu_0 h \quad (2)$$

$$BW = \frac{1}{\eta}\sqrt{\frac{L}{C}} \quad (3)$$

where, ε_0, and μ_0 are the permittivity and permeability of free space, respectively.

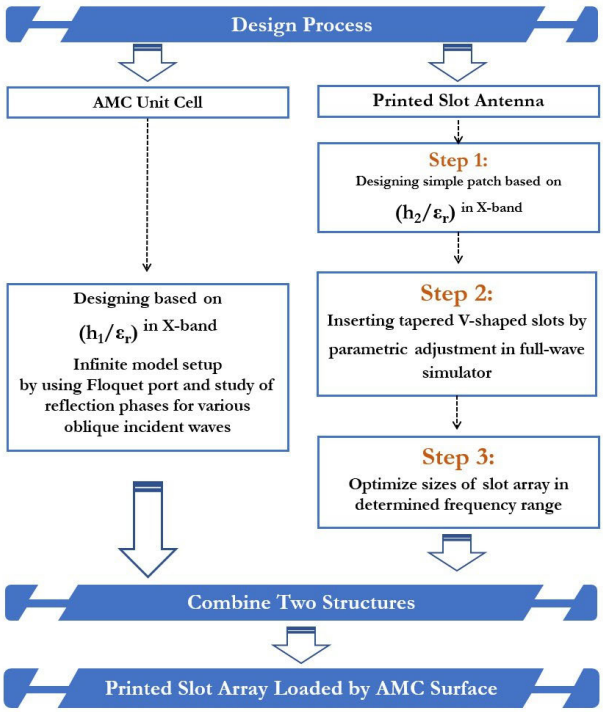

FIGURE 5. Diagram of the design procedure.

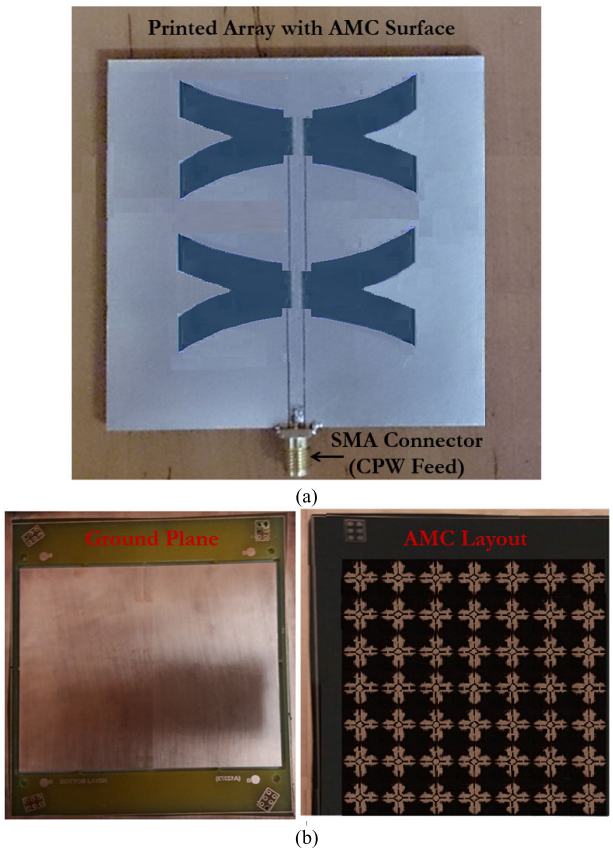

FIGURE 6. Images of fabricated layers (a) printed antenna with AMC reflector using feeding system (b).

The proposed AMC design evolution is provided in Fig. 2. It shows four steps to achieve the final design of the proposed

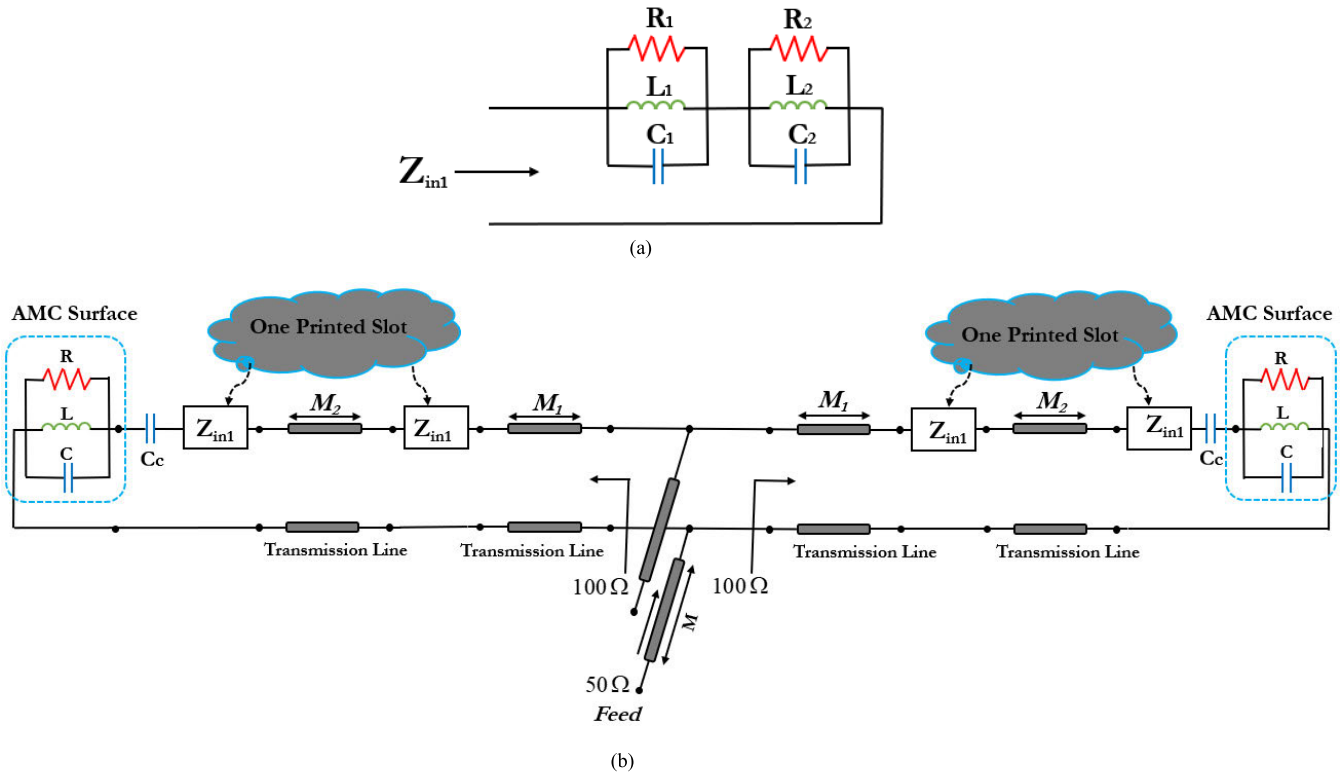

FIGURE 7. Equivalent transmission line model for antenna with AMC.

AMC. The reflection results of the AMCs and their effects on the printed antenna are investigated and compared in section IV.

B. PROPOSED PRINTED SLOT ARRAY

The geometry of the 2 × 2 printed slot array by applying the AMC structure is demonstrated in Fig. 3. Four tapered V-shaped slots are embedded on an FR4 substrate with 1.6 mm thickness. Beneath the printed antenna the 7×7 AMC surface is located. It is constructed of a substrate thickness (FR4) of h_1 to move the power to the printed array on the top layer. The dimensions of the width and length of tapered slots are 24 mm. These printed slots are placed on the substrate with dimensions of 79.1 × 80 mm^2. The 50-Ω CPW feeding system is applied from the side of the printed antenna with an SMA connector (see Fig. 6). The parameters of FR4 substrates select as thicknesses of $h_1 = 2.1$ mm, $h_2 = 1.6$ mm, $\varepsilon_r = 4.4$, and $\tan\delta = 0.02$. The 50-Ω CPW feed is considered with the width of the slot 0.3 mm and the width of the strip 3 mm to achieve the optimized design. The optimum length of $L_{cpw} = 30.4$ mm for the length of CPW is selected.

To optimize the final sizes and slots' lengths, parametric operations are performed in HFSS. Table 1 lists the sizes of the suggested design. The proposed printed slot array is realized based on tapered V-shaped slots for expanding the bandwidth with different resonances. The insertion of four tapered V-shaped slots into the printed antenna results in two resonances and consequently, the operating bandwidth can be widened. Meanwhile, according to Fig. 6, the proposed design is assembled by etching the AMC layer to the printed slot antenna and it is fed by 50-Ohm CPW from the center of the structure. It is noted that there is no gap layer between the AMC and the antenna.

The basic process of the design of the microstrip patch with the width (W) and length (L) is exhibited by the equations in [3]. In terms of the provided formulas in [3] at the X-frequency band, the basic width and length of the printed antenna are selected. In this design, dielectric constant substrate, $\varepsilon_r = 4.4$ is considered and for the simple patch at 9.7 GHz, the fundamental width and the length are regarded for height $h_2 = 1.6$ mm. Finally, the optimum sizes and lengths with the parametric studies are achieved. The proposed design evolution is provided in Fig. 4. It shows four steps to achieve the final design of the printed slot antenna with tapered V-shaped slots. The simulated results for four designs 1, 2, 3, and 4 are introduced in section IV.

The printed antenna is composed of the tapered slots with V-shaped arms. When two tapered V-shaped slots embed on the patch, an extra inductance and capacitance between the arms of the V-shaped patch are acquired to broad the bandwidth with two resonances.

Fig. 5 plots the structure of the design method. It demonstrates the comprehensive model with three steps to achieve an optimized printed design with enhanced features. At first, the novel wideband AMC design in 7.85-12.24 GHz (43.7%) for X-band operation is presented. In second stage, the printed slot antenna with the CPW feed in X-band (8.24-11.13 GHz) for wideband applications are introduced.

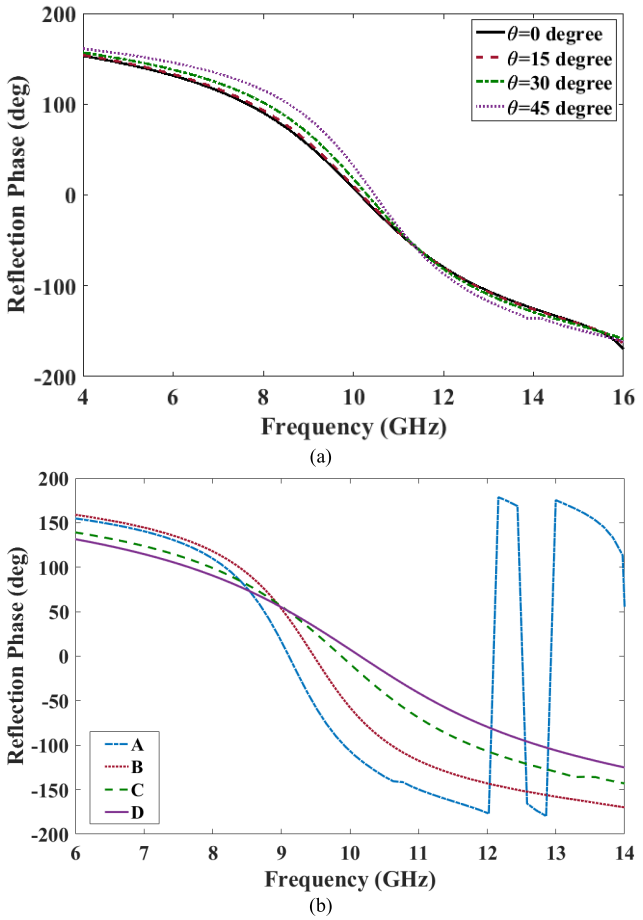

FIGURE 8. (a) Reflection phase of AMC (a) for θ in $\varphi = 0°$ and 90° (b) for four designs of A-D.

Finally, by combining and loading a novel wideband AMC reflector into wideband printed array an antenna with tapered V-shaped slots for wideband communications (4.47-13.32) is implemented.

Fig. 6 shows the photographs of the fabricated configurations of the antenna. The measured far-field setup and testing the radiation patterns of the antenna in the anechoic chamber is provided. A transmit (TX) antenna as a standard horn antenna is selected and the proposed antenna is located as a receiving (RX) antenna. The antenna (RX) is located at the far-field distance $2D^2/\lambda$ from the horn antenna and it is spined by a mechanical retainer for testing the radiation patterns in various directions. To achieve the power reception without variation, the amplifiers are used. To measure the S-parameters, the network analyzer of Agilent 8720C is used. The RF vector network analyzer operates in 50 MHz-20 GHz. Meanwhile, the gain of the antenna is tested in comparison with the reference horn antenna (G_{ref}) in terms of dBi. Also, the gain of the antenna ($G_{Relative}$) compared to the reference antenna is measured. Eventually, the aggregate of G_{ref} and $G_{Relative}$ for all frequencies is computed to attain the gain of the antenna. There is a little difference between the simulated and measured results of S-parameters, radiation patterns, gains, and efficiencies.

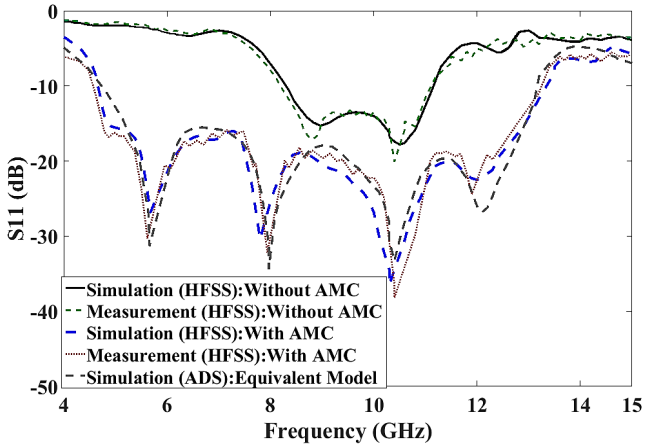

FIGURE 9. S-parameters of the structure.

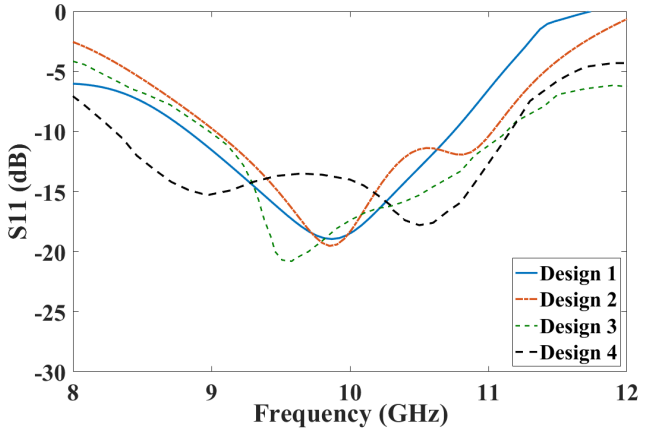

FIGURE 10. S-parameters of the antenna without AMC based on the design evolution of Fig. 4.

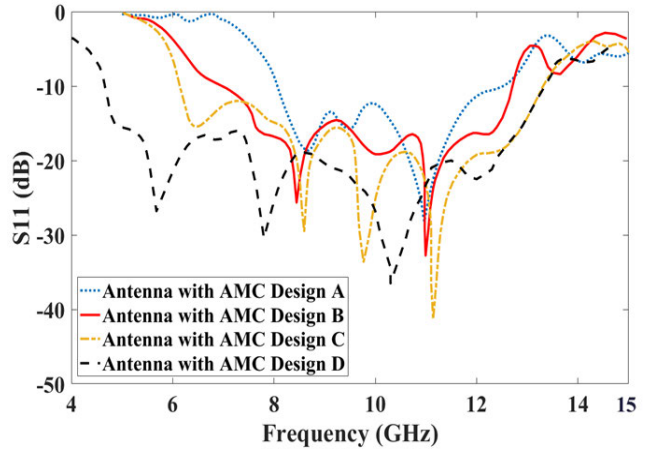

FIGURE 11. S-parameters of the antenna with AMC designs of A, B, C and D introduced in Fig. 2.

III. PROPOSED EQUIVALENT TRANSMISSION LINE MODEL

The proposed equivalent circuit model of the present design is depicted in Fig. 7. The circuit model of L_1C_1 for conventional

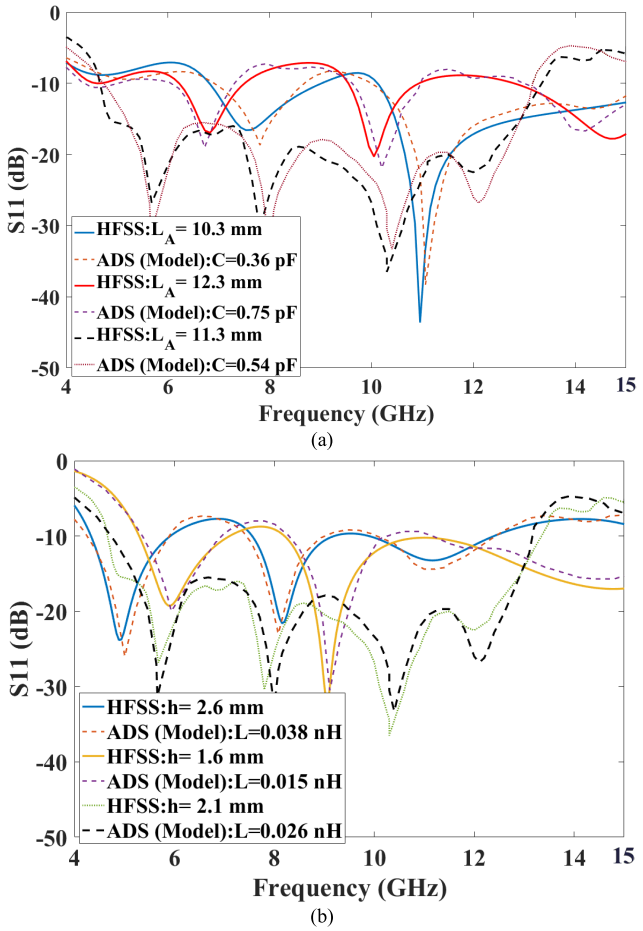

FIGURE 12. S-parameters of the design by variations of (a) patch sizes and capacitance in the RLC model of AMC unit cell (b) AMC height and inductance in the RLC model of AMC unit cell.

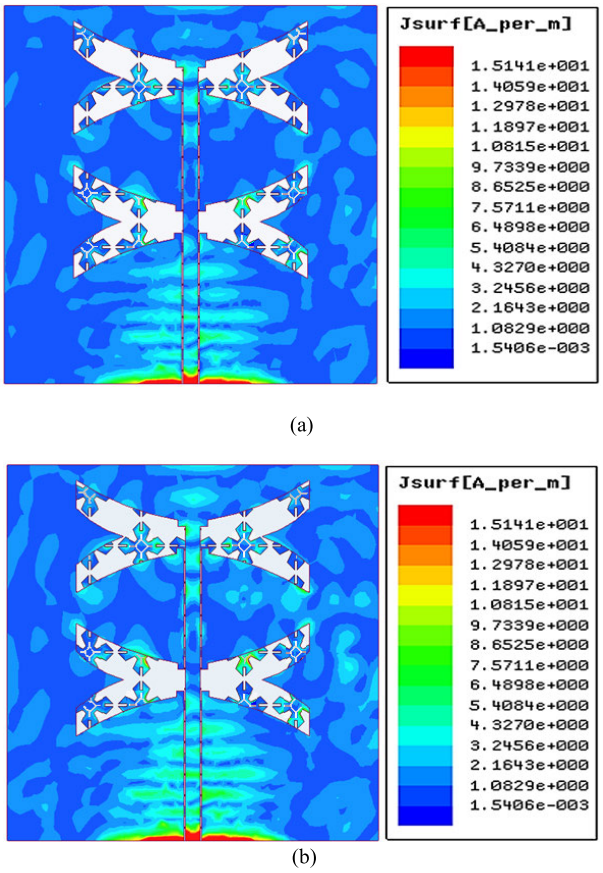

FIGURE 13. Surface current on the printed antenna at: (a) 5.7 (b) 10.4 GHz.

patch antenna is calculated [12] and [14]:

$$C_1 = \frac{\varepsilon_e \varepsilon_0 L_e W}{2h} \cos^{-2}\left(\frac{\pi y_0}{L}\right) \tag{4}$$

$$L_1 = \frac{1}{(2\pi f_r)^2 C_1} \tag{5}$$

$$R_1 = \frac{Q}{\omega C_1} \tag{6}$$

$$Q = \frac{c\sqrt{\varepsilon_e}}{4 f_r h} \tag{7}$$

$$C_c = \frac{-(C_1 + C_2) + \sqrt{((C_1 + C_2)^2 - 4C_1C_2(1 - 1/C_p^2))}}{2} \tag{8}$$

$$C_p = \frac{1}{\sqrt{Q_1 Q_2}} \tag{9}$$

$$C_2 = \mathrm{C}_1 \Delta C / (C_1 + \Delta C) \tag{10}$$

The proposed model of the array is introduced by utilizing the impedance model of wideband antennas [39]. It consists of two sections with the same 100-Ω impedance matching. Two same 100-Ω sections are connected in parallel to achieve 50-Ω input impedance. Accordingly, the V-shaped slots of a broadband antenna are modeled by multiple RLC parallel cells in series (Z_{in1}), as seen in Fig. 7 (a). The impedance Z_{in1} for one V-shaped slot through the transmission line of M_2 connects to another V-shaped slot branch. Two V-shaped slots of one 100-Ω branch are coupled with C_c to the AMC surface by an *RLC* resonator (see Fig. 7 (b)). The AMC surface is modelled by *LC* elements.

The all values of different elements with the method of moment (MOM) in the ADS are confirmed in terms of full-wave simulations. The optimized values of lumped elements in the proposed model are selected as: $R_1 = 50\ \Omega$, $C_1 = 2.63$ pF, $L_1 = 0.281$ nH, $R_2 = 50\ \Omega$, $C_2 = 2.73$ pF, $L_2 = 0.283$ nH, $R = 72\ \Omega$, $C = 0.54$ pF, $L = 0.026$ nH, $C_c = 0.24$ pF, $M = 30.4$ m, and $M_1 = 0.3$ mm,. The input impedance Z_{in} of the equivalent model is demonstrated as [12]:

$$Z_{in} = \sum_{k=1}^{n} \frac{j\omega . R_k . L_k}{R_k . (1 - \omega^2 . L_k . C_k) + j\omega . L_k} \tag{11}$$

The real part is considered simply the values of *RLC* parameters:

$$R_{in} = \sum_{k=1}^{n} \frac{R_k}{1 + R_k . (\frac{1}{L_k . 2\pi f} - C_k . 2\pi f)^2} \tag{12}$$

Based on the formula (12), the simulation outputs of the array design by HFSS are inserted into the input

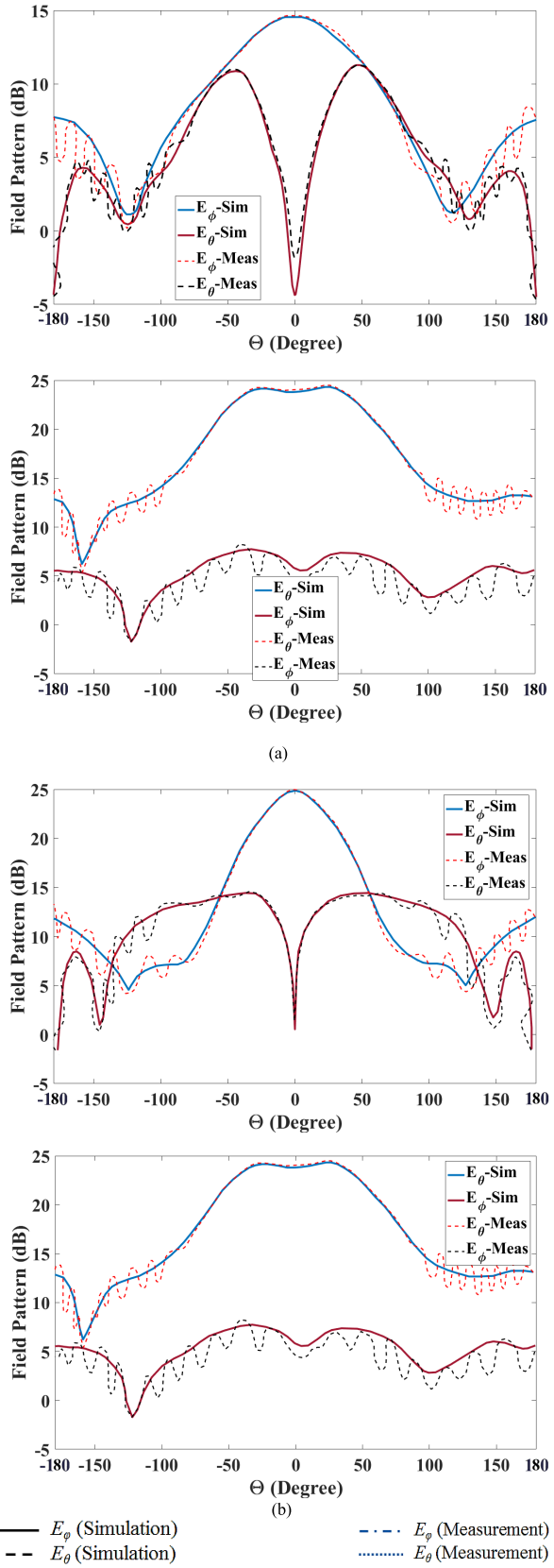

FIGURE 14. Radiation patterns of the design for co and cross-polarization (Measurement and simulation) (a) 5.7 GHz (b) 10.4 GHz.

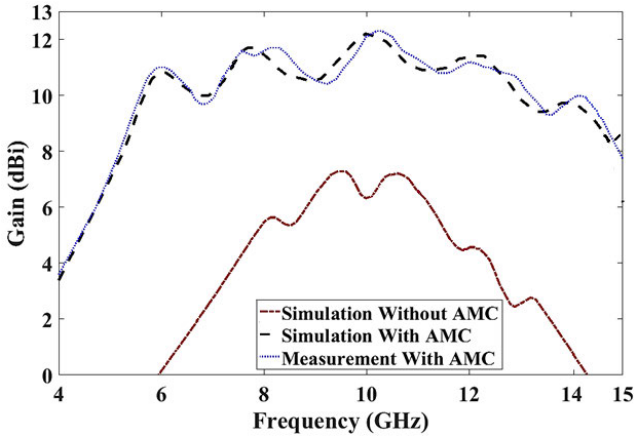

FIGURE 15. Gain of the proposed design.

impedance which acquired from the presented model. The optimized parameters are provided R_k, L_k, and C_k by using a least-square and curve-fitting techniques.

IV. SIMULATION AND EXPERIMENTAL RESULTS WITH DETAILED DISCUSSION

The finite element and Floquet theory are applied in HFSS to realize the reflection properties of the AMC unit cell. Fig. 8 (a) shows the AMC reflection phase by propagating the normal TE/TM waves. The simulated result of 7.85-12.24 GHz (43.7%) for normal TE/TM waves is obtained at the resonance of 10.14 GHz. Fig. 8 (a) displays the reflection phases of the AMC for various oblique incident waves (θ) from 0° to 45° in two polarization plates ($\varphi = 0°, 90°$). Also, the simulation results of the AMC design evolution based on Fig. 4 is displayed in Fig 8 (b). It reveals that four designs A, B, C, and D cover the bandwidths of 8.39-9.81, 8.56-10.42, 8.25-11.48, and 7.85-12.24 GHz, respectively.

The simulation and measurement S-parameters of the proposed printed antenna without AMC are provided in Fig. 9. The antenna without AMC is measured in 8.24-11.13 GHz (29.8%) for $S_{11} < -10$ dB. According to Fig. 9, the proposed antenna with the AMC surface displays a −10 dB bandwidth of 100% in 4.47-13.32 GHz from the measurement results. Therefore, the array with the AMC exhibits a bandwidth improvement of 70% versus the antenna without the AMC. The simulated S_{11} of the equivalent transmission line model achieves the operating band in 4.50-13.30 GHz, according to Fig. 9. Therefore, it is comprehended that the proposed equivalent circuit model with respect to the measured result predicts the wideband operation as well.

Fig. 10 demonstrates the results of the design evolution based on Fig. 4. For this purpose, four cases are considered in Fig. 4 to obtain the final design. According to Fig. 10, four designs 1, 2, 3, and 4 result in bandwidths of 8.8-10.7, 8.96-11, 8.92-11.12, and 8.24-11.13 GHz, respectively. The overall size of the antenna without the AMC

TABLE 2. Comparison of antenna design with other works.

Proposed design	Measured Impedance bandwidth (S_{11}≤-10 dB)	Total size (Width×Length×Height) and substrate	Maximum Gain	Applications	Design Complexity
Present work	4.47-13.32 GHz (100%)	79.1×80×3.7 mm^3 1.17λ_L×1.19λ_L×0.055λ_L Substrate: ε_r=4.4	12.3 dBi	wideband wireless Systems	Two layers
[8]	8.7-11.7 GHz, 11.9-14.6 GHz	37×70×1.6 mm^3 1.07λ_L×2.03λ_L×0.05λ_L Substrate: ε_r=4.3	9.15 dBi	RFID Applications	One layers (Using fractal EM band-gap fractal EBG)
[10]	8-9.25 GHz (14.5%)	96×96×1.6 mm^3 2.56λ_L×2.56λ_L×0.043λ_L Substrate: ε_r=4.3	7 dBi	X-band Applications	One layers (Closely-packed patch arrays based on decoupling structure of fractal cross-shaped EBG surface)
[24]	3–4.1 GHz (31%)	75×75×12.7 mm^3 0.75λ_L×0.75λ_L×0.127λ_L Substrate: ε_r=3.44	7.1 dBi	MIMO Systems	Two layers (Shorted V-shaped patches coupled by a bowtie dipole with 5×5 simple square AMC array)
[32]	1.64-1.94 GHz (16.8%)	50×70×25 mm^3 0.27λ_L×0.38λ_L×0.137λ_L Substrate: ε_r=4.4	6.5 dBi	Communication Systems	Two layers (Bow-tie printed antenna with 6×9 fractal simple circular AMC array)
[33]	6.9–7.9 GHz (13.5%)	76×76×7 mm^3 1.75λ_L×1.75λ_L×0.160λ_L Substrate: ε_r=2.2	13 dBi	Aerospace Applications	Two layers (Near-Zero-Index Metamaterial Lens Combined With mushroom type AMC)
[34]	2.2-2.72 GHz (18%)	67.5×67.5×4.5 mm^3 0.5λ_L×0.5λ_L×0.032λ_L Substrate: ε_r=3.5	5 dBi	Telemedicine Applications	Two layers (M-shaped antenna based on 3×3 Jerusalem Cross AMC array)
[35]	1.67-2.98 GHz (56.3%) 1.64-3.05 GHz (59%)	150×190×18.8 mm^3 0.82λ_L×1.04λ_L×0.103λ_L Substrate: ε_r=3.66	8.1 dBi	3G and 4G base stations	Two layers (Crossed-dipoles with wideband AMC reflector)
[36]	1.67-1.88 GHz (11.83%) 1.91-2.24 GHz (15.9%)	165×230×17.8 mm^3 0.918λ_L×1.28λ_L×0.099λ_L Substrate: ε_r=3.66	12.4-13.1 dBi	Base stations and Digital Cellular System	Two layers (Two parallel 1×4 sub-arrays with wideband AMC reflector)
[37]	3.3–3.7 GHz (11.7%) 5.4–5.87 GHz (9.1%)	62×62×5.5 mm^3 0.72λ_L×0.72λ_L×0.06λ_L Substrate: ε_r=1.2	7.2 dBi	Off-Body Communications	Two layers (Dual-band monopole antenna with AMC reflector)
[38]	5-6.20 GHz (20.5%)	34.4×34.4×4.016 mm^3 0.62λ_L×0.62λ_L×0.073λ_L Substrate: ε_r=2.2	7.6 dBi	WBAN Communications	Two layers (A Wearable CP Antenna with AMC)
[40]	5.88-6.1 GHz (3.7%)	40×40×3.2 mm^3 0.56λ_L×0.56λ_L×0.017λ_L Substrate: ε_r=3.35	3.9 dBi	Metallic Objects	Two layers (Rectangular patch antenna with slots and AMC reflector)
[41]	4.2-7.2 GHz (52.6%)	64×64×1.6 mm^3 0.71λ_L×0.71λ_L×0.044λ_L Substrate: ε_r=2.2	6.29 dBi	Wireless systems	Two layers (Reconfigurable ring-slot antenna and AMC reflector)
[42]	4.76–6.08 GHz (24.4%)	90×60×7 mm^3 1.44λ_0×0.46 λ_0×0.0512 λ_0 Substrate: ε_r=2	10.59 dBi	Medical and IoT Applications	Two layers (Printed antenna and AMC reflector)
[43]	4.63-6.08 GHz (25%)	140×140×6.8 mm^3 2.69λ_0×2.69λ_0×0.077λ_0 Substrate: ε_r=2.65	16.1 dBi	Wireless Communications	Three layers (Grid array layer, air gap, and the AMC surface)

is $2.17\lambda_L$, $2.19\lambda_L$ and $0.044\lambda_L$, respectively. Besides, the overall size of the antenna with the AMC is $1.17\lambda_L$, $1.19\lambda_L$, and $0.055\lambda_L$, respectively. Thus, by applying the AMC the reduction of the size of 109.4% achieves compared to the antenna without the AMC. Also, Fig. 10 compares the effect of V-shaped slots (Design 4) with respect to the tapered slots (Design 3) for enhancing the bandwidth and impedance matching.

Fig. 11 demonstrates the results of the S-parameters for the antenna with four AMC designs based on Fig. 2. According to Fig. 11, the printed antenna with four designs A, B, C, and D result in impedance bandwidths of 8.10-12.51, 6.94-12.71, 6.14-13.28, and 4.47-13.32 GHz, respectively.

The effect of the variations of patch sizes and the capacitance of C in the equivalent model for the unit cell in the AMC periodic surface is investigated in Fig. 12 (a). The simulation results are done by HFSS for the proposed design and ADS for the proposed equivalent model. As shown, by increasing the size of the unit cell and consequently, increasing the capacitance of C in the model, the bandwidth is enlarged until it achieves the optimum value of $C = 0.54$ pF. Also, the effect of the variations of height and the inductance of L in the equivalent model for the unit cell in AMC periodic surface is plotted in Fig. 12 (b). As shown, by passing the height of the unit cell and consequently, the inductance of L in the model, form the optimum value of $L = 0.026$ nH, the bandwidth decreases.

Fig. 13 displays the current distribution on the patch of the antenna at various resonances of 5.7 GHz and 10.4 GHz. At 5.7 GHz, the current density focuses on the feeding system and at 10.4 GHz it concentrates around tapered slots. The V-shaped slots are more effective on creating new resonances at higher frequencies. For this reason, the current density concentrates around the slots at 10 GHz compared to the lower frequency of 5.7 GHz. The measured and simulated radiation patterns for the suggested design in the xz- and yz-planes are exhibited in Fig. 14. According to Fig. 14, the radiation pattern at 10.4 GHz is more directional than that at 5.7 GHz. That is due to this fact that applying the AMC surface to printed slot antenna affet on lower frequencies by creating new resonances. Therefore, the radiation patterns have a wider beamwidth at lower frequencies. The maximum gain of the antenna with AMC whole the operational band is 12.3 dBi, according to Fig. 15. Hence, the gain at the frequency band is considerably improved.

The brief review of the proposed design in comparison to other works is listed in Table 2. It reveals notable features containing reduced size, wide bandwidth, and enhanced gain. The present design with respect to the other reports such as [8], [10], [24], [28], [32], [33], [34], [35], [36], [37], [38], [39], [40], [41], [42], and [43] introduces a wider bandwidth of 100% and an increased gain of 12.3 dBi with excellent impedance matching. In [41], an antenna of $64\times64\times1.6$ mm^3 includes 4.2-7.2 GHz (52.6%) and a gain of 6.29 dBi. Also, an array with EBG in [10] shows the bandwidth of 8-9.25 GHz (14.5%) with $96\times96\times1.6$ mm^3. Finally, the present study introduces a novel printed antenna and planar AMC for the C-band and the whole of the X-band for wideband communication systems.

V. CONCLUSION

The 2 × 2 printed slot array with tapered V-shaped slots loaded by a 7×7 AMC structure demonstrates the low-profile wideband antenna with -10 dB measured impedance bandwidth of 4.47-13.32 GHz (100%). The novel planar AMC design is presented to show a wide frequency band in 7.85-12.24 GHz (43.7%) with acceptable stability within the AMC bandwidth. The 2 × 2 printed array by loading the AMC compared to the antenna without AMC shows good impedance matching (-40 dB), good compactness (almost 110%) and improved bandwidth up to 100%. The total size of the printed design is selected 79.1 × 80 × 3.7 mm^3 ($1.17\lambda_L\times1.19\lambda_L\times0.055\lambda_L$). Moreover, the uni-directional radiation patterns and an enhanced gain of 12.3 dBi are acquired. Meanwhile, the proposed equivalent circuit model is introduced to foreseen the wideband operation for the input reflection coefficient as well. The obtained S_{11} of the proposed model shows the frequency band in 4.50-13.30 GH by utilizing the impedance model of the wideband antennas.

REFERENCES

[1] H. Wong, K. K. So, and X. Gao, "Bandwidth enhancement of a monopolar patch antenna with V-shaped slot for car-to-car and WLAN communications," *IEEE Trans. Veh. Technol.*, vol. 65, no. 3, pp. 1130–1136, Mar. 2016.
[2] L. Wen, S. Gao, Q. Luo, W. Hu, and Y. Yin, "Wideband dual circularly polarized antenna for intelligent transport systems," *IEEE Trans. Veh. Technol.*, vol. 69, no. 5, pp. 5193–5202, May 2020.
[3] L. Chi, Y. Qi, Z. Weng, W. Yu, and W. Zhuang, "A compact wideband slot-loop directional antenna for marine communication applications," *IEEE Trans. Veh. Technol.*, vol. 68, no. 3, pp. 2401–2412, Mar. 2019.
[4] T. Mondal, S. Maity, R. Ghatak, and S. R. B. Chaudhuri, "Compact circularly polarized wide-beamwidth fern-fractal-shaped microstrip antenna for vehicular communication," *IEEE Trans. Veh. Technol.*, vol. 67, no. 6, pp. 5126–5134, Jun. 2018.
[5] M. Hasan, I. Bahceci, M. A. Towfiq, T. M. Duman, and B. A. Cetiner, "Mode shift keying for reconfigurable MIMO antennas: Performance analysis and antenna design," *IEEE Trans. Veh. Technol.*, vol. 68, no. 1, pp. 320–334, Jan. 2019.
[6] X. Ge, H. Cheng, G. Mao, Y. Yang, and S. Tu, "Vehicular communications for 5G cooperative small-cell networks," *IEEE Trans. Veh. Technol.*, vol. 65, no. 10, pp. 7882–7894, Oct. 2016.
[7] T. Varum, J. N. Matos, P. Pinho, and R. Abreu, "Nonuniform broadband circularly polarized antenna array for vehicular communications," *IEEE Trans. Veh. Technol.*, vol. 65, no. 9, pp. 7219–7227, Sep. 2016.
[8] M. Alibakhshikenari, M. Khalily, B. S. Virdee, C. H. See, R. A. Abd-Alhameed, and E. Limiti, "Mutual coupling suppression between two closely placed microstrip patches using EM-bandgap metamaterial fractal loading," *IEEE Access*, vol. 7, pp. 23606–23614, 2019.
[9] D. Nashaat, H. A. Elsadek, E. A. Abdallah, M. F. Iskander, and H. M. Elhenawy, "Ultrawide bandwidth 2 ×2 microstrip patch array antenna using electromagnetic band-gap structure (EBG)," *IEEE Trans. Antennas Propag.*, vol. 59, no. 5, pp. 1528–1534, May 2011.
[10] M. Alibakhshikenari, B. S. Virdee, C. H. See, R. Abd-Alhameed, A. H. Ali, F. Falcone, and E. Limiti, "Study on isolation improvement between closely-packed patch antenna arrays based on fractal metamaterial electromagnetic bandgap structures," *IET Microw., Antennas Propag.*, vol. 12, no. 14, pp. 2241–2247, 2018.
[11] A. A. Althuwayb, "Enhanced radiation gain and efficiency of a metamaterial-inspired wideband microstrip antenna using substrate integrated waveguide technology for sub-6 GHz wireless communication systems," *Microw. Opt. Technol. Lett.*, vol. 63, no. 7, pp. 1892–1898, Jul. 2021.

[12] Q. Wu, Y. Zhou, and S. Guo, "An L-sleeve L-monopole antenna fitting a shark-fin module for vehicular LTE, WLAN, and car-to-car communications," *IEEE Trans. Veh. Technol.*, vol. 67, no. 8, pp. 7170–7180, Aug. 2018.
[13] K. D. Xu, H. Xu, Y. Liu, J. Li, and Q. H. Liu, "Microstrip patch antennas with multiple parasitic patches and shorting vias for bandwidth enhancement," *IEEE Access*, vol. 6, pp. 11624–11633, 2018.
[14] S.-H. Kim, J.-Y. Lee, T. T. Nguyen, and J.-H. Jang, "High-performance MIMO antenna with 1-D EBG ground structures for handset application," *IEEE Antennas Wireless Propag. Lett.*, vol. 12, pp. 1468–1471, 2013.
[15] H. Malekpoor and S. Jam, "Design, analysis, and modeling of miniaturized multi-band patch arrays using mushroom-type electromagnetic band gap structures," *Int. J. RF Microw. Comput.-Aided Eng.*, vol. 28, no. 6, pp. 1–13, 2018.
[16] X. Yang, Y. Liu, Y. Xu, and S. Gong, "Isolation enhancement in patch antenna array with fractal UC-EBG structure and cross slot," *IEEE Antennas Wireless Propag. Lett.*, vol. 16, pp. 2175–2178, 2017.
[17] M. Hamidkhani, H. Malekpoor, and H. Oraizi, "Oscillator phase-noise reduction using high-qsc active giuseppe peano fractal resonators," *IEEE Microw. Wireless Compon. Lett.*, vol. 29, no. 5, pp. 354–356, May 2019.
[18] D. Sievenpiper, L. Zhang, R. F. J. Broas, N. G. Alexopolous, and E. Yablonovitch, "High-impedance electromagnetic surfaces with a forbidden frequency band," *IEEE Trans. Microw. Theory Techn.*, vol. 47, no. 11, pp. 2059–2074, Nov. 1999.
[19] J. Deng, J. Li, L. Zhao, and L. Guo, "A dual-band inverted-F MIMO antenna with enhanced isolation for WLAN applications," *IEEE Antennas Wireless Propag. Lett.*, vol. 16, pp. 2270–2273, 2017.
[20] S. Rajagopal, G. Chennakesavan, D. R. P. Subburaj, R. Srinivasan, and A. Varadhan, "A dual polarized antenna on a novel broadband multilayer artificial magnetic conductor backed surface for LTE/CDMA/GSM base station applications," *AEU-Int. J. Electron. Commun.*, vol. 80, pp. 73–79, Oct. 2017.
[21] H. Lee and B. Lee, "Compact broadband dual-polarized antenna for indoor MIMO wireless communication systems," *IEEE Trans. Antennas Propag.*, vol. 64, no. 2, pp. 766–770, Feb. 2016.
[22] S. Ghosh, T. Tran, and T. Le-Ngoc, "Dual-layer EBG-based miniaturized multi-element antenna for MIMO systems," *IEEE Trans. Antennas Propag.*, vol. 62, no. 8, pp. 3985–3997, Aug. 2014.
[23] X. Liu, Y. Di, H. Liu, Z. Wu, and M. M. Tentzeris, "A planar windmill-like broadband antenna equipped with artificial magnetic conductor for off-body communications," *IEEE Antennas Wireless Propag. Lett.*, vol. 15, pp. 64–67, 2016.
[24] J. Zhu, S. Li, S. Liao, and Q. Xue, "Wideband low-profile highly isolated MIMO antenna with artificial magnetic conductor," *IEEE Antennas Wireless Propag. Lett.*, vol. 17, no. 3, pp. 458–462, Mar. 2018.
[25] A. Ghosh, V. Kumar, G. Sen, and S. Das, "Gain enhancement of triple-band patch antenna by using triple-band artificial magnetic conductor," *IET Microw., Antennas Propag.*, vol. 12, no. 8, pp. 1400–1406, 2018.
[26] N. Othman, N. A. Samsuri, M. K. A. Rahim, and K. Kamardin, "Low specific absorption rate and gain-enhanced meandered bowtie antenna utilizing flexible dipole-like artificial magnetic conductor for medical application at 2.4 GHz," *Microw. Opt. Technol. Lett.*, vol. 62, no. 12, pp. 3881–3889, Dec. 2020.
[27] R. C. Hadarig, M. E. de Cos, and F. Las-Heras, "Novel miniaturized artificial magnetic conductor," *IEEE Antennas Wireless Propag. Lett.*, vol. 12, pp. 174–177, 2013.
[28] J. Joubert, J. C. Vardaxoglou, W. G. Whittow, and J. W. Odendaal, "CPW-fed cavity-backed slot radiator loaded with an AMC reflector," *IEEE Trans. Antennas Propag.*, vol. 60, no. 2, pp. 735–742, Feb. 2012.
[29] H. Malekpoor and M. Shahraki, "Radiation properties improvement of 1 × 4 array of wideband printed antenna supported by AMC surface for vehicular MIMO systems," *Radio Sci.*, vol. 57, no. 6, pp. 1–18, Jun. 2022.
[30] H. Malekpoor and M. Hamidkhani, "Performance enhancement of low-profile wideband multi-element MIMO arrays backed by AMC surface for vehicular wireless communications," *IEEE Access*, vol. 9, pp. 166206–166222, 2021.
[31] J. Liu, J. Y. Li, J. J. Yang, Y. X. Qi, and R. Xu, "AMC-loaded low-profile circularly polarized reconfigurable antenna array," *IEEE Antennas Wireless Propag. Lett.*, vol. 19, pp. 1276–1280, 2020.
[32] Y. Zhong, G. Yang, and L. Zhong, "Gain enhancement of bow-tie antenna using fractal wideband artificial magnetic conductor ground," *Electron. Lett.*, vol. 51, no. 4, pp. 315–317, Feb. 2015.
[33] J. P. Turpin, Q. Wu, D. H. Werner, B. Martin, M. Bray, and E. Lier, "Near-zero-index metamaterial lens combined with AMC metasurface for high-directivity low-profile antennas," *IEEE Trans. Antennas Propag.*, vol. 62, no. 4, pp. 1928–1936, Apr. 2014.
[34] H. R. Raad, A. I. Abbosh, H. M. Al-Rizzo, and D. G. Rucker, "Flexible and compact AMC based antenna for telemedicine applications," *IEEE Trans. Antennas Propag.*, vol. 61, no. 2, pp. 524–531, Feb. 2013.
[35] M. Li, Q. L. Li, B. Wang, C. F. Zhou, and S. W. Cheung, "A low-profile dual-polarized dipole antenna using wideband AMC reflector," *IEEE Trans. Antennas Propag.*, vol. 66, no. 5, pp. 2610–2615, May 2018.
[36] M. Li, Q. Li, B. Wang, C. Zhou, and S. Cheung, "A miniaturized dual-band base station array antenna using band notch dipole antenna elements and AMC reflectors," *IEEE Trans. Antennas Propag.*, vol. 66, no. 6, pp. 3189–3194, Jun. 2018.
[37] H. Yang, X. Liu, Y. Fan, and L. Xiong, "Dual-band textile antenna with dual circular polarizations using polarization rotation AMC for off-body communications," *IEEE Trans. Antennas Propag.*, vol. 70, no. 6, pp. 4189–4199, Jun. 2022.
[38] Y. B. Chaouche, M. Nedil, I. B. Mabrouk, and O. M. Ramahi, "A wearable circularly polarized antenna backed by AMC reflector for WBAN communications," *IEEE Access*, vol. 10, pp. 12838–12852, 2022.
[39] I. Pele, A. Chousseaud, and S. Toutain, "Simultaneous modeling of impedance and radiation pattern antenna for UWB pulse modulation," in *Proc. IEEE AP-S Int. Symp.*, vol. 2, Jun. 2004, pp. 1871–1874.
[40] W. Luo and P. Wang, "A compact UHF-RFID tag antenna with embedded AMC for metallic objects," *IEEE Antennas Wireless Propag. Lett.*, vol. 22, no. 4, pp. 873–877, Apr. 2023.
[41] J. Huang, M. Shirazi, and X. Gong, "A new arraying technique for band-switchable and polarization-reconfigurable antenna arrays with wide bandwidth," *IEEE Open J. Antennas Propag.*, vol. 3, pp. 1025–1040, 2022.
[42] A. B. Dey, S. Kumar, W. Arif, and J. Anguera, "Elastomeric textile substrates to design a compact, low-profile AMC-based antenna for medical and IoT applications," *IEEE Internet Things J.*, vol. 10, no. 6, pp. 4952–4969, Mar. 2023.
[43] G. Hao, S. Xing, Y. Liu, W. Zhang, and Y. Gao, "A broadband compact micro strip grid array antenna backed by an AMC reflector," *Int. J. RF Microw. Comput.-Aided Eng.*, vol. 32, no. 11, p. e23375, Nov. 2022.

HOSSEIN MALEKPOOR (Member, IEEE) was born in Iran, in 1985. He joined the Faculty of Engineering, Arak University, in 2017, where he is currently an Assistant Professor with the Department of Electrical Engineering. His research interests include different antennas designs, wideband microstrip antennas for UWB applications and wireless communication, the analysis of antenna with equivalent circuit models, phased array antennas, designing the periodic structures, such as EBGs, AMCs, and FSSs, and antenna design with EBG and AMC surfaces.

MEHDI HAMIDKHANI was born in Isfahan, Iran, in 1985. He received the B.E. degree in electrical engineering from Yazd University, Iran, in 2007, the M.Sc. degree in electrical engineering from the Iran University of Science and Technology (IUST), Tehran, Iran, in 2010, and the Ph.D. degree in electrical engineering from Shiraz University, Shiraz, Iran, in 2016.

He is currently a Assistant Professor with the Dolatabad Branch, Islamic Azad University, Isfahan. His current research interests include RF microwave circuits, antenna, wireless networks, and the IoT.